

Structure and Properties of Carbonyl-Coordinated Ruthenium(II) and Osmium(II) Porphyrin Dimers Bridged by Aza Ligands

Chika Bando, Atsushi Furukawa, Kiyoshi Tsuge, Kazumi Takaishi, Yoichi Sasaki, and Taira Imamura*

Division of Chemistry, Graduate School of Science, Hokkaido University, Sapporo 060-0810

Received February 22, 2007; E-mail: timamura@sci.hokudai.ac.jp

Carbonyl-coordinated ruthenium(II) and osmium(II) porphyrin dimers bridged with aza ligands, $[\{M(\text{por})(\text{CO})_2\}_2(\text{BL})]$ ($M = \text{Ru}^{\text{II}}, \text{Os}^{\text{II}}$; por = ttp (5,10,15,20-tetra-*p*-tolylporphyrinato dianion), oep (2,3,7,8,12,13,17,18-octaethylporphyrinato dianion); BL = pz (pyrazine), bpy (4,4'-bipyridine), dabco (1,4-diazabicyclo[2,2,2]octane)), were prepared and characterized, and their structures were determined by using single-crystal X-ray crystallography. The metal–metal distances of the pz-, bpy-, and dabco-bridged dimers in $[\{M(\text{por})(\text{CO})_2\}_2(\text{BL})]$ were about 7.1–7.3, 11.5, and 7.3–7.4 Å, respectively. From electrochemical measurements, the first oxidation waves of the ruthenium and osmium porphyrin dimers with the pz and dabco, except the Ru–oep systems, were split, although the first oxidation in the Ru complexes occurs at the porphyrin rings and in the Os complexes occurs at the metal centers. The extent of the potential splits at the first oxidation processes, which reflects magnitude of the intramolecular redox interactions, was in the orders: ttp > oep and Os (metal oxidation) > Ru (ring oxidation), and dabco \geq pz \gg bpy.

Multiporphyrin assemblies have been extensively studied in order to obtain more information on functional materials,¹ such as catalysts,² receptors,³ and diverse photophysical devices.^{4,5} In such assemblies, arrangement of porphyrin subunits that control intramolecular interaction plays a key role in the emergence of the above functionality. For intramolecular interaction, close arrangement of two porphyrins is required. One way to accomplish this is to use metal porphyrins with coordinating groups, such as pyridyl groups.^{5,6} Introduction of metal ions into pyridylporphyrins has afforded a variety of self-assembled oligomers, which frequently show intramolecular interactions as observed by electrochemical and UV–vis spectral measurements. For example, unique slipped-cofacial dimers, which are formed by the introduction of ruthenium(II) ions into 2-pyridylporphyrin, show a remarkable intramolecular interaction.⁷ The two central ruthenium ions of the dimers having pyridine as axial ligands are electrochemically oxidized at the first process step-by-step (potential split ≈ 300 mV), giving a stable mixed-valence state that shows a unique coupling phenomenon between ground-state molecular vibrations and low-energy electronic transition (electron-molecular vibration coupling).^{7,8} The other way for effective arrangement is the use of bridging ligands,^{9–14} that is, the shish-kebab approach.¹³ Linear chain-like porphyrin oligomers thus constructed by bridging two metalloporphyrin subunits ($\text{Fe}^{\text{II}}, \text{Ru}^{\text{II}},$ and Os^{II}) with aza ligands, such as pz,¹⁵ also show distinct intramolecular redox interactions, that is, large splits of the redox waves at the metal centers. The extent of the splits follows the order of Os > Ru > Fe in metals and pz > bpy, except dabco systems.¹⁴ However, aza ligand-bridged molecular ruthenium oep–porphyrin dimers having CO as an axial ligand, which are very similar in structure to the dimer unit constituting above the chain-like polymers, shows no distinct splits in the cyclic voltammograms of the first electrochemical oxi-

dation process of the porphyrin ring, that is, two one-electron transfers proceeded almost simultaneously.¹⁶

These results motivated us to investigate in detail the properties of discrete ruthenium(II) and osmium(II) porphyrin dimers with pz, bpy, or dabco as a bridging ligand and CO as an axial ligand illustrated in Fig. 1, focusing especially on their intramolecular interactions, which can be evaluated by electrochemical or UV–vis spectral measurements. Effects of different metal centers, porphyrin rings, and bridging ligands on the intramolecular interaction are interesting subjects, because the first oxidations of monomeric ruthenium(II) and

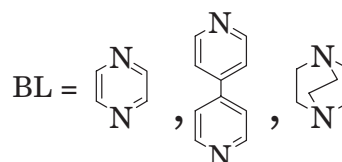
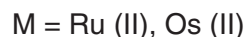
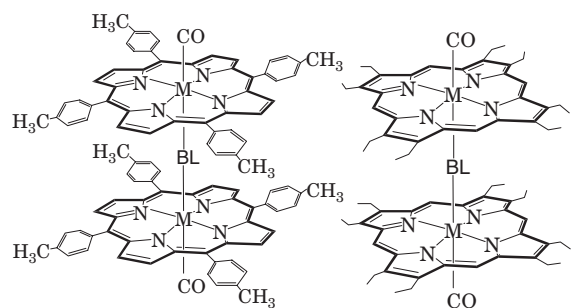


Fig. 1. Carbonyl-coordinated metalloporphyrin dimers.

osmium(II) porphyrins with a CO axial ligand occur at the porphyrin rings¹⁷ and metal centers,¹⁸ respectively, and the metal porphyrin dimers with a dabco bridging ligand show no intramolecular redox interactions, as far as we know.

In the present work, a variety of aza ligand-bridged ruthenium(II) and osmium(II) porphyrin dimers with CO as an axial ligand, $[\{M(\text{por})(\text{CO})\}_2(\text{BL})]$, were prepared, characterized, and studied with respect to intramolecular interactions by using electrochemical and UV–vis spectral measurements. The structures of eight dimers were determined by single-crystal X-ray crystallography. In the pz and dabco bridging systems, almost all ruthenium and osmium porphyrin dimers, except Ru–oep systems, clearly showed electrochemical and UV–vis spectral intramolecular interactions.

Experimental

Instrumentation. IR spectra (KBr pellet) were measured with a JASCO FT/IR-660 Plus. UV–vis spectra were recorded on a Hitachi U-3000 spectrophotometer. ¹H NMR spectra were recorded on a JEOL model JNM-EX270 spectrometer. Mass spectra were measured with a JEOL JMS-HX110 for FAB-MS and a JEOL JMS-700TZ for ESI-MS at the Center for Instrumental Analysis in Hokkaido University. Cyclic voltammograms and differential pulse voltammograms were recorded with a Hokutodenko model HZ-3000 voltammetry analyzer at 20 °C with a scan rate of 100 mV s⁻¹ and a BAS model CV-50, respectively. The working and the counter electrodes were a platinum disk electrode (inside diameter of 1.6 mm) and a platinum wire, respectively. The same electrolyte (0.1 M TBA(PF₆)) and solvent (CH₂Cl₂) were used in order to compare the potentials, unless otherwise specified. The sample solutions were deoxygenated by a stream of argon. The reference electrode was Ag/AgCl. The redox potentials obtained were corrected for a ferrocenium/ferrocene couple (Fc⁺/Fc = 0.000 V). The numbers of transferred electrons were determined by the wave heights of CV and DPV.

X-ray Crystallography. The single crystals of the present dimer complexes suitable for X-ray analysis were obtained from CH₂Cl₂–pentane or CHCl₃–pentane solutions. Structure data were collected on a Rigaku AFC-8S diffractometer or a Rigaku AFC-7R diffractometer with a Mercury CCD Area detector using graphite-monochromated Mo K α radiation ($\lambda = 0.71073 \text{ \AA}$) at 153 K and processed using the CrystalClear software program.¹⁹ Final cell parameters were obtained from a least-square analysis of reflections with $I > 10\sigma(I)$. The crystal structures were solved by direct methods and expanded using Fourier and difference Fourier techniques. All calculations were performed using the CrystalStructure²⁰ and SHELXL-97 software.²¹

For the ttp complexes, non-hydrogen atoms in the complex molecules were refined anisotropically, and the hydrogen atoms were fixed at the calculated positions, except those of disordered bridging ligands. The crystals of the ttp complexes contained crystal solvents, which were disordered partially and refined with isotropic displacement parameters. The hydrogen atoms of the crystal solvents were not included in the calculations.

Two oep complexes afforded isomorphous crystals. The porphyrin ring was disordered around the C₄ axis over two positions. The hydrogen atoms were not included in the calculations of the oep complexes, because the disorder caused positional overlap of the hydrogen and carbon atoms.

Crystallographic data have been deposited with Cambridge Crystallographic Data Centre: Deposition numbers CCDC-

635612–635619. Copies of the data can be obtained free of charge via <http://www.ccdc.cam.ac.uk/conts/retrieving.html> (or from the Cambridge Crystallographic Data Centre, 12, Union Road, Cambridge, CB2 1EZ, UK; Fax: +44 1223 336033; e-mail: deposit@ccdc.cam.ac.uk).

Materials. Silica gel, alumina (neutral, activity III), and CH₂Cl₂ as an eluant were used for column chromatography. The monomer complexes with ruthenium(II) ion or osmium(II) ion, that is, [Ru(tp)(CO)(CH₃OH)],²² [Ru(tp)(CO)(py)],²³ [Os(tp)(CO)(py)],²⁴ [Os(tp)(CO)(mpy)], and [Os(oep)(CO)(py)], were prepared by reference to the reported methods as the source of corresponding porphyrin dimers and in order to compare their properties. The preparation methods for [Os(tp)(CO)(py)] and [Os(tp)(CO)(mpy)] are given as examples.

[Os^{II}(tp)(CO)(py)]. The complex was prepared from [Os(tp)(CO)]. [Os(tp)(CO)] was prepared from H₂(tp) and Os₃(CO)₁₂ by using the reported methods (yield: 33%).²⁴ A CH₂Cl₂ solution (100 mL) containing [Os(tp)(CO)] (100 mg, 110 μ mol) and pyridine (0.5 mL, 6.2 mmol) was stirred for 1 h at room temperature and evaporated to dryness. The resulting solid was chromatographed using silica gel to give a single band. The eluent was concentrated and the resulting solid was recrystallized from CH₂Cl₂–pentane. The crystals obtained were collected by filtration and dried for 3 h at 80 °C under reduced pressure (yield: 62.5 mg, 57%).

Anal. Calcd for C₅₄H₄₁N₅OOS: C, 67.13; H, 4.28; N, 7.25%. Found C, 66.96; H, 4.32; N, 7.36%. ¹H NMR (CDCl₃, 270 MHz): δ H_{CH₃} 2.67 (s, 12H), H_m 7.48 (ddd, 8H), H_o 7.98 (ddd, 8H), H _{β} 8.50 (s, 8H), H_{py} 1.60 (dt, 2H), 5.23 (t, 2H), 6.12 (t, 1H). FAB-MS: 967 m/z [M]⁺.

[Os^{II}(tp)(CO)(mpy)]. The complex was prepared by the same method as that for the [Os(tp)(CO)(py)] (yield: 59%), except using mpy in place of py.

Anal. Calcd for C₅₅H₄₃N₅OOS: C, 67.39; H, 4.42; N, 7.15%. Found: C, 67.30; H, 4.37; N, 7.33%. ¹H NMR (CDCl₃, 270 MHz): δ H_{CH₃} 2.67 (s, 12H), H_m 7.48 (ddd, 8H), H_o 7.98 (ddd, 8H), H _{β} 8.49 (s, 8H), H_{mpy} 1.22 (s, 3H), 1.46 (dd, 2H), 5.03 (dd, 2H). FAB-MS: 981 m/z [M]⁺.

[{Ru^{II}(tp)(CO)}₂(pz)]. The complex was prepared by using a reported method.²⁵ To the CH₂Cl₂ (50 mL) solution of [Ru(tp)(CO)(CH₃OH)] (41 mg, 49 μ mol), pz (1.9 mg, 24 μ mol) in a CH₂Cl₂ solution was slowly added. The solution was stirred for 3 h and evaporated to dryness. The products were isolated by column chromatography using silica gel. The first band eluted with CH₂Cl₂ was concentrated, followed by recrystallization of the residue from CH₂Cl₂–pentane and dried in vacuo for 3 h (yield: 21 mg, 50%).

Anal. Calcd for C₁₀₂H₇₆N₁₀O₂Ru₂: C, 73.10; H, 4.57; N, 8.36%. Found: C, 72.70; H, 4.25; N, 8.32%. ¹H NMR (CDCl₃, 270 MHz): δ H_{tolyl} 2.68 (s, 24H), H_m 7.37 (s, 16H), H_o 7.63 (dd, 16H), H _{β} 8.32 (s, 16H), H_{pz} -0.61 (s, 4H). FAB-MS: 1675 m/z [M]⁺.

[{Ru^{II}(tp)(CO)}₂(bpy)]. The dimer was prepared by a method similar to that of [{Ru^{II}(tp)(CO)}₂(pz)] and dried in air (yield: 56%).

Anal. Calcd for C₁₀₈H₈₀N₁₀O₂Ru₂: C, 74.04; H, 4.60; N, 8.00%. Found: C, 74.07; H, 4.64; N, 8.09%. ¹H NMR (CDCl₃, 270 MHz): δ H_{tolyl} 2.63 (s, 24H), H_m 7.39 (dd, 16H), H_o 7.81 (dd, 16H), H _{β} 8.45 (s, 16H), H_{bpy} 1.21 (d, 4H), 4.36 (d, 4H).

[{Ru^{II}(tp)(CO)}₂(dabco)]. The complex was prepared by a method similar to that for [{Os^{II}(tp)(CO)}₂(dabco)] (vide infra). A CH₂Cl₂ solution of dabco (11 mg, 99 μ mol) was added to a

CH_2Cl_2 (50 mL) solution of $[\text{Ru}(\text{ttp})(\text{CO})(\text{CH}_3\text{OH})]$ (61 mg, 73 μmol). The solution was stirred for 30 min, and the solvent was evaporated to dryness. The resulting solid was suspended in methanol. After filtration, the solid was thoroughly washed with methanol and dried under reduced pressure at 100 °C for 3 h (yield: 42 mg, 67%).

Anal. Calcd for $\text{C}_{104}\text{H}_{84}\text{N}_{10}\text{O}_2\text{Ru}_2$: C, 73.13; H, 4.96; N, 8.20%. Found: C, 72.38; H, 5.05; N, 8.22%. $^1\text{H NMR}$ (CDCl_3 , 270 MHz): δ H_{tolyl} 2.70 (s, 24H), H_m 7.44 (q, 16H), H_o 7.59 (ddd, 16H), H_β 8.29 (s, 16H), H_{dabco} -5.43 (s, 12H). FAB-MS: 1708.5 m/z [M] $^+$.

$[\{\text{Ru}^{\text{II}}(\text{oe}p)(\text{CO})\}_2(\text{pz})]$ and $[\{\text{Ru}^{\text{II}}(\text{oe}p)(\text{CO})\}_2(\text{dabco})]$.¹⁶ These dimers were prepared for a comparison to other dimers by methods similar to those above for the corresponding ttp complexes and characterized.

$[\{\text{Os}^{\text{II}}(\text{ttp})(\text{CO})\}_2(\text{pz})]$. To a CH_2Cl_2 solution of $[\text{Os}(\text{ttp})(\text{CO})]$ (80 mg, 90 μmol), a CH_2Cl_2 solution of pz (6.0 mg, 75 μmol) was slowly added. The solution was stirred for 30 min and column-chromatographed using silica gel. The first band was collected and the solvent was evaporated. The residue was recrystallized from CH_2Cl_2 -pentane. The product in the solid state was dried in vacuo for 3 h at 50 °C under reduced pressure (yield: 53 mg, 63%).

Anal. Calcd for $\text{C}_{102}\text{H}_{76}\text{N}_{10}\text{O}_2\text{Os}_2$: C, 66.07; H, 4.13; N, 7.55%. Found: C, 65.78; H, 4.26; N, 7.88%. $^1\text{H NMR}$ (CDCl_3 , 270 MHz): δ H_{CH_3} 2.64 (s, 24H), H_m 7.34 (s, 16H), H_o 7.63 (dd, 16H), H_β 8.23 (s, 16H), H_{pz} -0.56 (s, 4H). FAB-MS: 1855 m/z [M] $^+$.

$[\{\text{Os}^{\text{II}}(\text{ttp})(\text{CO})\}_2(\text{bpy})]$. The bpy dimer was prepared by a similar method to that for the pz dimer. $[\text{Os}(\text{ttp})(\text{CO})]$ (40 mg, 45 μmol) was dissolved in CH_2Cl_2 (60 mL). To the solution, a CH_2Cl_2 solution containing bpy (8.7 mg, 56 μmol) was slowly added. The mixed solution was agitated for 5 h, and the solvent was evaporated to dryness. The resulting solid was again dissolved in a small amount of CH_2Cl_2 for purification by column chromatography using silica gel. The first band was collected and concentrated to give the dimer complex. The complex was recrystallized from CH_2Cl_2 -pentane and dried in vacuo for 3 h (yield: 25 mg, 57%).

Anal. Calcd for $\text{C}_{108}\text{H}_{80}\text{N}_{10}\text{O}_2\text{Os}_2$: C, 67.20; H, 4.18; N, 7.26%. Found: C, 67.29; H, 4.30; N, 7.30%. $^1\text{H NMR}$ (CDCl_3 , 270 MHz): δ H_{CH_3} 2.62 (s, 24H), H_m 7.39 (dd, 16H), H_o 7.79 (ddd, 16H), H_β 8.34 (s, 16H), H_{bpy} 1.21 (d, 4H), 4.43 (d, 4H). FAB-MS: 1930 m/z [M] $^+$.

$[\{\text{Os}^{\text{II}}(\text{ttp})(\text{CO})\}_2(\text{dabco})]$. The preparation of the dabco complex was initially tried by a method similar to the pz complex. However, different from the pz system, purification by column chromatography was unsuccessful, because of strong adsorption of dabco onto silica gel. Column chromatography gave only a mixture of the target dimer and the original $[\text{Os}(\text{ttp})(\text{CO})]$. After many trials of purification, the crude product was purified without column chromatography. Namely, the mixture obtained by a method similar to the pz dimer was suspended in methanol, filtered through a fritted filter, and washed thoroughly with methanol to give directly the dabco dimer (yield: 52 mg, 59%).

The properties of $[\{\text{Os}^{\text{II}}(\text{ttp})(\text{CO})\}_2(\text{dabco})]$ are a little different in several points from those of $[\{\text{Os}^{\text{II}}(\text{ttp})(\text{CO})\}_2(\text{pz})]$ and $[\{\text{Os}^{\text{II}}(\text{ttp})(\text{CO})\}_2(\text{bpy})]$, the behavior on columns, lower solubility in CH_2Cl_2 , and instability in CHCl_3 . A CHCl_3 solution of the dabco dimer gave unknown precipitates, when it was left to stand for one day. Extra addition of CHCl_3 to the solution causes no dissolution of the precipitates. However, the CH_2Cl_2 solution of the dabco complex gave no such precipitation in a few days.

Anal. Calcd for $\text{C}_{104}\text{H}_{84}\text{N}_{10}\text{O}_2\text{Os}_2$: C, 66.22; H, 4.49; N, 7.43%. Found: C, 65.77; H, 4.60; N, 7.51%. $^1\text{H NMR}$ (CDCl_3 , 270 MHz): δ H_{CH_3} 2.70 (s, 24H), H_m 7.44 (dd, 16H), H_o 7.57 (dd, 16H), H_β 8.19 (s, 16H), H_{dabco} -5.28 (s, 12H). FAB-MS: 1886.6 m/z [M] $^+$.

$[\{\text{Os}^{\text{II}}(\text{oe}p)(\text{CO})\}_2(\text{pz})]$. A CH_2Cl_2 solution of pz (3.1 mg, 39 μmol) was slowly added to a CH_2Cl_2 solution of $[\text{Os}(\text{oe}p)(\text{CO})]$ (40 mg, 53 μmol). The solution was stirred for 2 h and column-chromatographed using silica gel. The first band was collected and the solvent was evaporated. The residue was crystallized from CH_2Cl_2 -pentane. The product in the solid state was dried in vacuo for 3 h at 50 °C under reduced pressure (yield: 30 mg, 72%).

Anal. Calcd for $\text{C}_{78}\text{H}_{92}\text{N}_{10}\text{O}_2\text{Os}_2$: C, 59.22; H, 5.86; N, 8.55%. Found: C, 58.97; H, 5.99; N, 8.83%. $^1\text{H NMR}$ (CDCl_3 , 270 MHz): δ H_{meso} 9.11 (s, 8H), $\text{H}_{\text{C}_{\text{H}_2\text{CH}_3}}$ 3.65 (q, 32H), $\text{H}_{\text{CH}_2\text{CH}_3}$ 1.63 (t, 48H), H_{pz} -1.55 (s, 4H). ESI-MS: 1582 m/z (M^+).

$[\{\text{Os}^{\text{II}}(\text{oe}p)(\text{CO})\}_2(\text{bpy})]$. This complex was prepared by a method similar to that for $[\{\text{Os}^{\text{II}}(\text{oe}p)(\text{CO})\}_2(\text{pz})]$ (yield: 70%).

Anal. Calcd for $\text{C}_{84}\text{H}_{96}\text{N}_{10}\text{O}_2\text{Os}_2$: C, 60.84; H, 5.83; N, 8.45%. Found: C, 60.84; H, 5.46; N, 8.38%. $^1\text{H NMR}$ (CDCl_3 , 270 MHz): δ H_{meso} 9.40 (s, 8H), $\text{H}_{\text{bpy,NCH}_2}$ 3.97 (d, 4H), $\text{H}_{\text{C}_{\text{H}_2\text{CH}_3}}$ 3.74 (q, 32H), $\text{H}_{\text{CH}_2\text{CH}_3}$ 1.73 (t, 48H), $\text{H}_{\text{bpy,NCH}_2}$ 0.35 (d, 4H). ESI-MS: 1658 m/z [M] $^+$.

$[\{\text{Os}^{\text{II}}(\text{oe}p)(\text{CO})\}_2(\text{dabco})]$. This complex was prepared by a method similar to that for $[\{\text{Os}^{\text{II}}(\text{ttp})(\text{CO})\}_2(\text{dabco})]$ (yield: 34%).

Anal. Calcd for $\text{C}_{80}\text{H}_{100}\text{N}_{10}\text{O}_2\text{Os}_2$: C, 59.53; H, 6.23; N, 8.66%. Found: C, 58.94; H, 6.23; N, 8.66%. $^1\text{H NMR}$ (CDCl_3 , 270 MHz): δ H_{meso} 9.08 (s, 8H), $\text{H}_{\text{C}_{\text{H}_2\text{CH}_3}}$ 3.63 (q, 32H), $\text{H}_{\text{CH}_2\text{CH}_3}$ 1.55 (t, 48H), H_{dabco} -5.28 (s, 12H). ESI-MS: 1614 m/z [M] $^+$.

Results and Discussion

Structure. The crystal structures of $[\{\text{M}(\text{ttp})(\text{CO})\}_2(\text{pz})]$, $[\{\text{M}(\text{ttp})(\text{CO})\}_2(\text{bpy})]$, $[\{\text{M}(\text{ttp})(\text{CO})\}_2(\text{dabco})]$, and $[\{\text{M}(\text{oe}p)(\text{CO})\}_2(\text{pz})]$ were determined by X-ray structure analysis. Structures and crystal data of the complexes are shown in Fig. 2 and Table 1, respectively. The porphyrin rings were almost planar in the complexes. The deviations of 24 atoms of each porphyrin ring from their mean planes were less than 0.23 Å. The M–M separations reflect the size of the bridging ligands. In case of smaller bridging ligands, such as pz and dabco, the M–M separations were 7.1–7.3 Å, whereas for the bpy complexes the separations were 11.4–11.5 Å. The bridging bpy adopted a planar structure in $[\{\text{M}(\text{ttp})(\text{CO})\}_2(\text{bpy})]$.

The structures of the ttp complexes consisted of a pair of parallel porphyrin rings with a bridging aza-ligand, except for $[\{\text{Ru}(\text{ttp})(\text{CO})\}_2(\text{pz})]$, in which two porphyrin rings were tilted from each other by 37°. Other than this pz complex, the Ru– and Os–ttp complexes with the same bridging ligands adopted quite similar structures and had a crystallographical or substantial mirror plane horizontal to the OC–M...M–CO axis. Namely, the two ttp rings in each complex adopted an eclipsed form along the OC–M...M–CO axis to bring the tolyl groups in the pz- and dabco-bridged complexes close together. Although the close contact of tolyl ligands is unfavorable due to steric hindrance, the mutual arrangement between the bridging ligands and the porphyrin rings resulted in the eclipsed form. The closest H...H distances²⁶ between the neighboring tolyl groups of upper and lower porphyrins were 3.01 and 2.70 Å in the pz and dabco complexes, respectively, which are still slightly larger than twice of the van der Waals radius of H

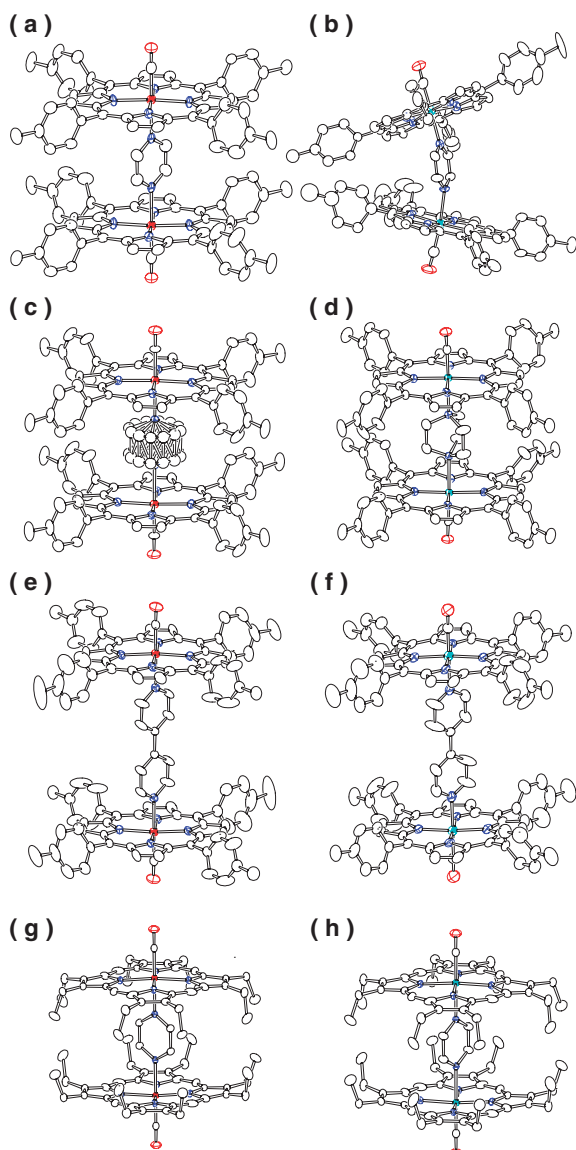


Fig. 2. ORTEP drawings of $[\{M(\text{por})(\text{CO})_2(\text{BL})\}]$ with 50% thermal ellipsoid. Hydrogen atoms are omitted for clarity. (a) $[\{\text{Os}(\text{tp})(\text{CO})_2(\text{pz})\}]$, (b) $[\{\text{Ru}(\text{tp})(\text{CO})_2(\text{pz})\}]$, (c) $[\{\text{Os}(\text{tp})(\text{CO})_2(\text{dabco})\}]$, (d) $[\{\text{Ru}(\text{tp})(\text{CO})_2(\text{dabco})\}]$, (e) $[\{\text{Os}(\text{tp})(\text{CO})_2(\text{bpy})\}]$, (f) $[\{\text{Ru}(\text{tp})(\text{CO})_2(\text{bpy})\}]$, (g) $[\{\text{Os}(\text{oep})(\text{CO})_2(\text{pz})\}]$, (h) $[\{\text{Ru}(\text{oep})(\text{CO})_2(\text{pz})\}]$. In the oep complexes, one set of oep pairs is depicted (see text).

atom, and the overall structures appear to be determined by the interaction between the porphyrin rings and the bridging ligands. The pz and bpy planes bisected the N–M–N angle in the porphyrin rings to avoid the steric repulsion between porphyrin rings and hydrogen atoms of the bridging ligands. In case of the dabco-bridged Os complex, dabco was disordered. However, in the Ru complex, dabco was fixed in a position where less steric repulsion between the porphyrin rings and the bridging dabco ligand is achieved. To avoid the steric repulsion with the bridging dabco ligand, both the upper and lower porphyrin rings adopted an eclipsed form with mirror symmetry. The regular structures of each molecule also bring about

the tight packing in the crystal lattice (Fig. S1). The sticking tolyl groups support the molecular arrangements by touching ones of the neighboring molecules. The eclipsed arrangement of porphyrins in the crystals should result from these weak steric interactions.

As an exceptional case, $[\{\text{Ru}(\text{tp})(\text{CO})_2(\text{pz})\}]$ had a highly distorted structure. The dihedral angles between the porphyrin rings and the pz deviated from ideal 90° by $15.9(2)$ and $19.8(2)^\circ$, whereas the deviation of $\angle\text{N}(\text{por})\text{--M--N}(\text{pz})$ from ideal 90° was only $0.1\text{--}7.5^\circ$. The larger deviation of the dihedral angles between the pz and the porphyrin rings than $\angle\text{N}(\text{por})\text{--M--N}(\text{pz})$ shows that the pz plane tilted to the M–N bond to cause the distorted structure of $[\{\text{Ru}(\text{tp})(\text{CO})_2(\text{pz})\}]$.

Although the bridging pz ligand can rotate around the M...M axis even in this distorted form, the pz was not disordered in the structure. Like a cover board for the open space formed between the two porphyrin subunits, the plane of pz faced toward the inside of the wedge-shape structure as shown in Fig. 2b. Rotation of the bridging pz ligand around the M...M axis from the observed position brings two of the four hydrogen atoms of pz close to the porphyrin rings, leading to destabilization of the Ru–N(pz) bonds. In the crystal lattice, these distorted molecules were arranged so that pinched and open sides alternated in order to minimize the steric repulsion between the molecules. The weak interactions between the porphyrin rings and the bridging ligand and among the neighboring molecules in the crystal lattice resulted in the regular molecular structures of the five ttp complexes or the distorted structure of $[\{\text{Ru}(\text{tp})(\text{CO})_2(\text{pz})\}]$.

The pz-bridged oep complexes $[\{M(\text{oep})(\text{CO})_2(\text{pz})\}]$ afforded isomorphous crystals with an $I4/mmm$ space group. The complexes occupy the $4/mmm$ position with the OC–M...M–CO axis on the 4-fold axis. The porphyrin rings were disordered over two positions around the 4-fold axis with $20.5(2)$ and $20.5(1)^\circ$ rotation for Os and Ru complexes, respectively. As shown by the local $4/mmm$ symmetry, $[\{M(\text{oep})(\text{CO})_2(\text{pz})\}]$ had a pair of parallel porphyrin rings as observed for the ttp complexes. The eight ethyl groups on an oep ring were all folded to the inner part of the molecule to make a “capsule” with two CO ligands sticking out as shown in Fig. 3. These capsules were piled up creating a body-centered lattice. Because of the disorder, there were two possible arrangements of the upper and the lower porphyrin rings, namely, eclipsed and twisted ones. However, the eclipsed form should be favorable as in the case of the ttp complexes, because the ring arrangements are determined by the steric repulsion between bridging ligands and porphyrins. In the eclipsed form, the closest distance between C atoms in neighboring methyl group was $3.35(1)$ and $3.381(9)$ Å for Os and Ru complexes,²⁷ respectively, which again is very close but not too close to cause the strong repulsion.²⁸ The molecular structures of $[\{M(\text{oep})(\text{CO})_2(\text{pz})\}]$ in the crystals are the results of the weak interactions as discussed for the ttp complexes.

UV–Vis Spectra and CO Stretches. UV–vis spectra of the porphyrin dimers were similar to those of the corresponding monomers. However, the Soret bands were shifted to wavelengths shorter than those of $[\text{Os}(\text{tp})(\text{CO})(\text{py})]$, $[\text{Os}(\text{oep})(\text{CO})(\text{py})]$, or $[\text{Ru}(\text{tp})(\text{CO})(\text{py})]$ by several nanometers, accompanied by a decrease in molar extinction coefficients per

Table 1. Crystal Data and Metal–Metal Distances^{a)}

	[[Os(tp)(CO)] ₂ (pz)] •5.9CH ₂ Cl ₂	[[Os(tp)(CO)] ₂ - (bpy)]•3CH ₂ Cl ₂	[[Os(tp)(CO)] ₂ (dabco)] •0.4CH ₂ Cl ₂ •1.2C ₅ H ₁₂	[[Os(oep)- (CO)] ₂ (pz)]	[[Ru(tp)(CO)] ₂ - (pz)]•1.5C ₅ H ₁₂	[[Ru(tp)(CO)] ₂ - (bpy)]•6CHCl ₃	[[Ru(tp)(CO)] ₂ (dabco)] •4.6CH ₂ Cl ₂ •1.3C ₅ H ₁₂	[[Ru(oep)- (CO)] ₂ (pz)]
Formula	C _{105.9} H _{87.8} N ₁₀ ⁻ O ₂ Os ₂ Cl _{11.8}	C ₁₁₁ H ₈₆ N ₁₀ O ₂ ⁻ Os ₂ Cl ₆	C _{110.4} H _{99.2} N ₁₀ ⁻ O ₃ Os ₂ Cl _{0.8}	C ₇₈ H ₉₂ N ₁₀ ⁻ O ₂ Os ₂	C _{109.5} H ₉₄ ⁻ N ₁₀ O ₂ Ru ₂	C ₁₁₄ H ₈₆ N ₁₀ ⁻ O ₂ Ru ₂ Cl ₁₈	C _{115.1} H _{108.8} N ₁₀ ⁻ O ₂ Ru ₂ Cl _{9.2}	C ₇₈ H ₉₂ N ₁₀ O ₂ Ru ₂
Mw	2331.3	2185.1	2006.8	1582.1	1784.2	1911.2	2192.5	1403.8
Crystal syst	monoclinic	triclinic	tetragonal	tetragonal	triclinic	triclinic	monoclinic	tetragonal
Space group	<i>I2/m</i>	<i>P</i> $\bar{1}$	<i>I4/m</i>	<i>I4/mmm</i>	<i>P</i> $\bar{1}$	<i>P</i> $\bar{1}$	<i>P2</i> ₁ / <i>m</i>	<i>I4/mmm</i>
<i>a</i> /Å	14.200(6)	10.29(2)	14.6695(5)	13.3293(5)	16.638(6)	16.74(2)	14.165(1)	13.3347(8)
<i>b</i> /Å	23.701(4)	13.38(5)	14.6695(5)	13.3293(5)	16.995(6)	19.57(3)	23.936(2)	13.3347(8)
<i>c</i> /Å	15.659(4)	19.12(4)	23.456(2)	19.9145(11)	18.502(5)	10.76(1)	15.648(1)	19.965(1)
α /deg	90	100.03(6)	90	90	68.312	110.30(2)	90	90
β /deg	91.220(5)	95.56(6)	90	90	70.79(1)	94.914(4)	91.120(2)	90
γ /deg	90	95.52(6)	90	90	82.75(1)	112.53(1)	90	90
<i>V</i> /Å ³	5269(3)	2536(1)	5047.5(5)	3538.2(3)	4590(2)	2955(6)	5304.5(8)	3550.1(4)
<i>Z</i>	2	1	2	2	2	1	2	2
Crystal dimensions /mm ³	0.25 × 0.5 × 0.5	0.1 × 0.175 × 0.875	0.175 × 0.25 × 0.25	0.16 × 0.15 × 0.21	0.13 × 0.08 × 0.18	0.05 × 0.08 × 0.58	0.4 × 0.55 × 0.63	0.61 × 0.32 × 0.30
λ (Mo K α)/Å	0.7107	0.7107	0.7107	0.7107	0.7107	0.7107	0.7107	0.7107
<i>T</i> /K	153	153	153	153	153	153	153	153
No. of total data collected	9109	12074	17101	9795	19790	10052	24341	10038
No. of independent rfln ($F^2 > 2\sigma(F^2)$)	3931	8611	2780	1170	10221	4891	10402	1197
<i>R</i> 1 ($F^2 > 2\sigma(F^2)$)	0.065	0.050	0.037	0.025	0.086	0.099	0.0940	0.038
<i>wR</i> 2 (all)	0.192	0.1440	0.107	0.062	0.217	0.288	0.2660	0.100
Metal–metal/Å	7.2626(7)	11.4791(3)	7.3444(3)	7.1676(3)	7.1387(9)	11.448(1)	7.3339(7)	7.1719(6)

a) CCDC No.: CCDC 635612–635619.

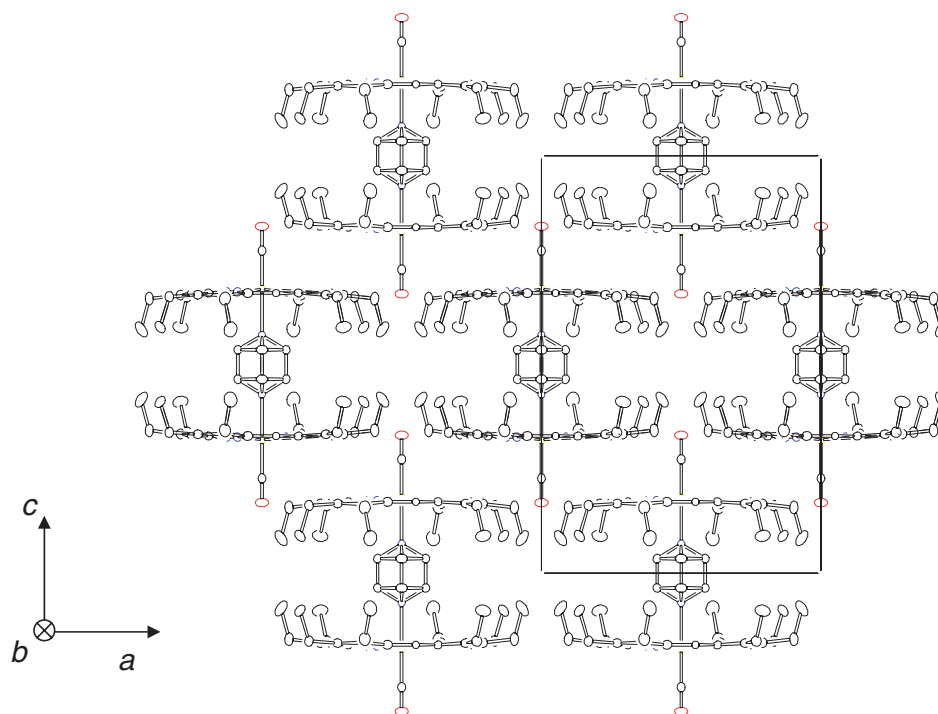


Fig. 3. The crystal packing of $[\{\text{Os}(\text{oep})(\text{CO})_2(\text{pz})\}]$ molecules. The other set of disordered oep is omitted for clarity.

Table 2. UV-Vis and IR Data of Osmium and Ruthenium Porphyrins

Complex	$\lambda_{\text{max}}/\text{nm}$ ($\epsilon/10^4 \text{ M}^{-1} \text{ cm}^{-1}/\epsilon$ per subunit/ $10^4 \text{ M}^{-1} \text{ cm}^{-1}$) in CH_2Cl_2	$\nu_{\text{CO}}/\text{cm}^{-1}$
$[\{\text{Os}(\text{ttp})(\text{CO})_2(\text{pz})\}]$	404 (52.7/26.4), 520 (3.2/1.6)	1932
$[\{\text{Os}(\text{ttp})(\text{CO})_2(\text{bpy})\}]$	408 (53.1/26.5), 520 (3.4/1.7)	1932
$[\{\text{Os}(\text{ttp})(\text{CO})_2(\text{dabco})\}]$	405 (57.8/28.9), 517 (3.1/1.5)	1923
$[\text{Os}(\text{ttp})(\text{CO})(\text{py})]$	410 (30.1), 521 (1.8)	1920
$[\text{Os}(\text{ttp})(\text{CO})(\text{mpy})]$	410, 520	1917
$[\{\text{Os}(\text{oep})(\text{CO})_2(\text{pz})\}]$	388 (40.3/20.2), 508 (2.32/1.16), 537 (3.28/1.64)	1915
$[\{\text{Os}(\text{oep})(\text{CO})_2(\text{bpy})\}]$	391 (55.4/27.7), 508 (2.67/1.34), 538 (3.94/1.97)	1914
$[\{\text{Os}(\text{oep})(\text{CO})_2(\text{dabco})\}]$	389 (49.7/24.9), 507 (2.14/1.07), 538 (3.45/1.73)	1905
$[\text{Os}(\text{oep})(\text{CO})(\text{py})]$	394 (32.4), 510 (1.29), 541 (2.23) ^{a)}	1902 ^{b)}
$[\{\text{Ru}(\text{ttp})(\text{CO})_2(\text{pz})\}]$	408, 531, 566	1959
$[\{\text{Ru}(\text{ttp})(\text{CO})_2(\text{bpy})\}]$	410, 532, 568	1960
$[\{\text{Ru}(\text{ttp})(\text{CO})_2(\text{dabco})\}]$	408, 530, 564	1952
$[\text{Ru}(\text{ttp})(\text{CO})(\text{py})]$	413, 533, 566	1950

a) Ref. 29. b) Ref. 30, Nujol mull.

each constituent porphyrin subunit with considerable broadening, as listed in Table 2, which reflects the presence of intramolecular interactions. The blue shifts are due to the excitonic interaction between two porphyrin rings facing each other, as explained by the Kasha model.³¹ In every series of $[\{\text{Os}(\text{ttp})(\text{CO})_2(\text{BL})\}]$, $[\{\text{Os}(\text{oep})(\text{CO})_2(\text{BL})\}]$, and $[\{\text{Ru}(\text{ttp})(\text{CO})_2(\text{BL})\}]$, the smallest blue shifts were observed in the bpy complexes with the largest metal-metal distance (ca. 11.5 Å) suggesting very weak interactions. This is consistent with Ru-octaphenylporphyrin-bpy dimers which show no interactions.³² The CO stretches of all the complexes were observed at wave numbers a little larger than the corresponding pyridine monomer complexes.

¹H NMR Spectra. There were no essential differences in

¹H NMR profiles between the ruthenium porphyrin dimers and the corresponding osmium porphyrin dimers. The ¹H NMR signals of the bridging pz in $[\{\text{M}(\text{por})(\text{CO})_2(\text{pz})\}]$ were observed at around -0.6 and around -1.5 ppm as a single peak, respectively, which were significantly shifted upfield compared to the corresponding resonance shifts of non-coordinating pz observed at 8.6 ppm. The dabco-bridging ligands of $[\{\text{M}(\text{por})(\text{CO})_2(\text{dabco})\}]$ also showed a single peak at around -5.3 and -5.3 (Os complex)–-6.3 (Ru-complex) ppm, respectively, and a peak for free base of dabco was observed at 2.8 ppm. On the other hand, $[\{\text{M}(\text{ttp})(\text{CO})_2(\text{bpy})\}]$ gave two signals, e.g., the $[\{\text{Os}(\text{ttp})(\text{CO})_2(\text{bpy})\}]$ complex had signals at 1.21 and 4.43 ppm ascribed to α and β protons of the bpy ligand. The upfield shifts were about 6.3 ppm from those of

Table 3. Redox Potentials (E /mV) and Potential Differences (ΔE)^{a)}

Complex	Os ₂ ^{III,III} /Os ₂ ^{II,II}	ΔE	por ₂ (+,+)/por ₂ (0,0) ^{f)}
[[Os(oep)(CO)] ₂ (pz)]	179 [1], 259 [1]	80	830 [2]
[[Os(oep)(CO)] ₂ (bpy)]	83 [2]	≈0	827 [2]
[[Os(oep)(CO)] ₂ (dabco)]	148 [2] (broad)	≈50 ^{e)}	831 [2]
[[Os(tp)(CO)] ₂ (pz)]	364 [1], 438 [1]	74	917 [2]
[[Os(tp)(CO)] ₂ (bpy)]	249 [2]	≈0	897 [2]
[[Os(tp)(CO)] ₂ (dabco)]	280 [1], 387 [1]	107	927 [2]
	por ₂ (+,+)/por ₂ (0,0) ^{f)}	ΔE	Ru ₂ ^{III,III} /Ru ₂ ^{II,II}
[[Ru(oep)(CO)] ₂ (pz)] ^{b)}	240 [2]	≈0	690 [2]
[[Ru(oep)(CO)] ₂ (pz)] ^{c)}	265 [2]	≈0	699 [2]
[[Ru(oep)(CO)] ₂ (pz)] ^{d)}	275 [2]	≈0	746 [2]
[[Ru(oep)(CO)] ₂ (bpy)] ^{b)}	170 [2]	≈0	690 [2]
[[Ru(oep)(CO)] ₂ (dabco)] ^{b)}	210 [2]	≈0	750 [2]
[[Ru(oep)(CO)] ₂ (dabco)] ^{c)}	205 [2]	≈0	660 [2]
[[Ru(oep)(CO)] ₂ (dabco)] ^{d)}	265 [2]	≈0	806 [2]
[[Ru(tp)(CO)] ₂ (pz)]	390 [1], 450 [1]	60	830 [2]
[[Ru(tp)(CO)] ₂ (bpy)]	300 [2]	≈0	800 [2]
[[Ru(tp)(CO)] ₂ (dabco)]	350 [1], 420 [1]	70	840 [2]

a) Potentials were obtained by DPV for the CH₂Cl₂ solutions containing 0.1 M TBA(PF₆) as an electrolyte and corrected for Fc⁺/Fc (0.000 V) at 20 °C, unless otherwise specified. The numbers in brackets are the numbers of transferred electron. b) Ref. 16. The reported values are the half-wave potentials ($E_{1/2} = (E_{pa} - E_{pc})/2$) obtained by CV for the CH₂Cl₂ solutions with 0.1 M TBAP at 25 °C and corrected for Fc⁺/Fc (0.000 V). c) This work. The values are the half-wave potentials ($E_{1/2}$) obtained by CV measurements using 0.1 M TBAP. d) This work. The values are the half-wave potentials ($E_{1/2}$) obtained by CV measurements using 0.1 M TBA(PF₆). e) This value was estimated from almost a linear relationship between the ΔE values and the FWHM (full width at half maximum from the top in mV) values obtained for the dimer complexes which gave separated peaks at the first oxidation processes of DPV measurements (Fig. S2). f) The plus and zero charges indicate the site of oxidation, not the formal valence.

a free-base of the bpy ligand, indicating smaller shielding effects due to elongation of the distance between two porphyrins compared to the pz and dabco systems. These signal patterns demonstrate that all of the porphyrin dimer structures with two facing porphyrins are maintained in solution, though from X-ray crystallography, in the structure of [[Ru(tp)(CO)]₂(pz)], the two porphyrin subunits were not parallel.

Electrochemistry. As described above, in carbonyl-coordinated osmium porphyrin complexes, the first oxidation occurs at the metal centers,¹⁸ whereas in carbonyl ruthenium porphyrin complexes, the first oxidation proceeds at the porphyrin rings.¹⁷ Interplanar distances longer than 7 Å exclude any direct porphyrin ring–porphyrin ring interaction, because through-space interactions are negligible for interorbital separations greater than 3 Å.^{33a,34} First, the reported ruthenium porphyrin systems of [[Ru(oep)(CO)]₂(BL)] were reinvestigated by CV and DPV under the same experimental conditions as those using TBAP as an electrolyte.¹⁶ The results were essentially the same with the reported data. Namely, no clear splits were observed in the first oxidation process as shown in Table 3. The use of TBA(PF₆) as an electrolyte gave the same result. However, the DPV of [[Ru(tp)(CO)]₂(pz)] showed a broad wave at around 400 mV as shown in Fig. 4, suggesting the Ru complex is oxidized stepwise during the first process. Each of two waves composing the broad wave was estimated

to be 390 and 450 mV as listed in Table 3. The difference (ca. 60 mV) corresponds to the comproportionation constant (K_c) of ca. 11, indicating the presence of a weak intramolecular redox interaction. CV and DPV of the osmium porphyrin dimers of [[Os(por)(CO)]₂(pz)] more clearly showed the stepwise two-redox waves at their first oxidation processes of the metal centers. On the other hand, the oxidation waves for [[Os(tp)(CO)]₂(pz)] observed at around 400 and 900 mV were ascribed to the oxidations of osmium ion and porphyrin rings respectively.^{18,29} The former broad oxidation wave at around 400 mV corresponds two reversible one-electron oxidations, whereas the second oxidation of the porphyrin rings involves one-step two-electron transfers. The potential difference of the two stepwise oxidations at the first oxidation process was determined to be 74 mV ($K_c = 19$). An unexpected result was obtained in both of the ruthenium and osmium dabco systems. Although intramolecular redox interaction was expected to be too weak to be detected in the dabco systems, because the bridging ligand does not resonate and the distance between two osmium ions is larger than those of the pz systems, the dabco systems showed a split in the first processes. For example, from the CV and DPV data of [[Os(tp)(CO)]₂(dabco)], the osmium ions were oxidized at 280 and 387 mV, and the porphyrin rings were oxidized at 927 mV at the second process. The split in the one-electron stepwise ox-

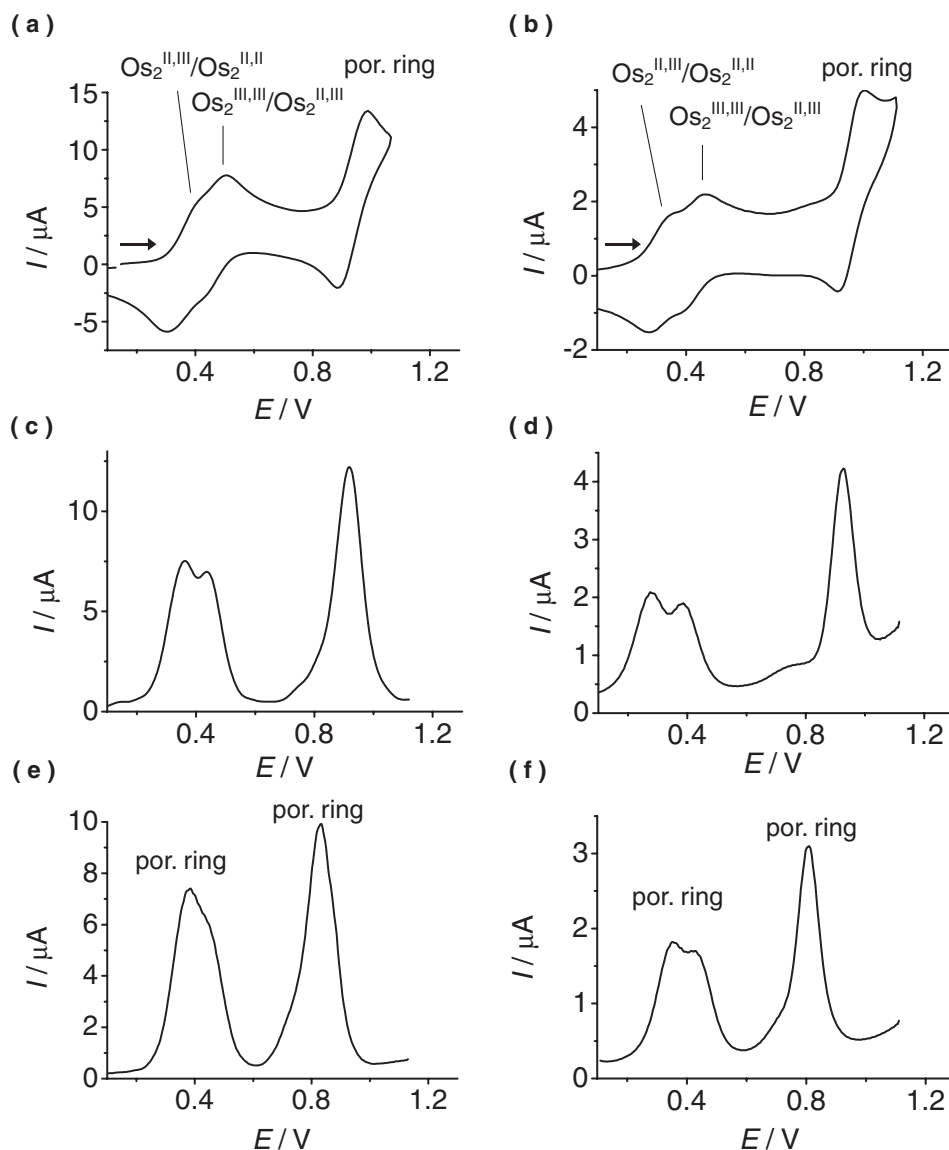


Fig. 4. Voltammograms of selected metalloporphyrin dimers by CV and DPV. Potentials were corrected for a ferrocenium/ferrocene couple ($\text{Fc}^+/\text{Fc} = 0.000 \text{ V}$). (a) $[\{\text{Os}(\text{tp})(\text{CO})_2(\text{pz})\}]$ (CV), (b) $[\{\text{Os}(\text{tp})(\text{CO})_2(\text{dabco})\}]$ (CV), (c) $[\{\text{Os}(\text{tp})(\text{CO})_2(\text{pz})\}]$ (DPV), (d) $[\{\text{Os}(\text{tp})(\text{CO})_2(\text{dabco})\}]$ (DPV), (e) $[\{\text{Ru}(\text{tp})(\text{CO})_2(\text{pz})\}]$ (DPV), (f) $[\{\text{Ru}(\text{tp})(\text{CO})_2(\text{dabco})\}]$ (DPV).

idation at the first process was 107 mV. This value (107 mV) corresponds to 69 of K_c and is a little larger than those of the $[\{\text{Os}(\text{tp})(\text{CO})_2(\text{pz})\}]$ ($K_c = 19$) and $[\{\text{Os}(\text{oep})(\text{CO})_2(\text{pz})\}]$ ($K_c = 24$) systems. In all of the $[\{\text{Os}(\text{por})(\text{CO})_2(\text{bpy})\}]$ systems as well as the $[\{\text{Ru}(\text{por})(\text{CO})_2(\text{bpy})\}]$ systems, there were no splits in the first oxidation process of the osmium ions as suggested by the large distance between two osmium ions determined by X-ray crystallography.

Effects of Porphyrin Rings and Bridging Ligands. In the series of porphyrin dimers having the same metal ions and porphyrin rings, the oxidation potentials increased in the order of $\text{pz} > \text{dabco} > \text{bpy}$ as shown in Table 3. The Creutz-Taube ion, in which pz bridges two ruthenium units, shows a strong intramolecular redox interaction through bonds.³⁵ This strong interaction results from the intramolecular interaction between πd orbitals of ruthenium ion and π^* orbitals of pz. This theory suggests that both the pz and bpy bridging complexes poten-

tially show intramolecular interactions, but the dabco bridging complex without a π -conjugated system shows only weak intramolecular redox interaction through bonds or no interaction. In practice, compared to the dimers of triruthenium complexes bridged by pz (split $\approx 400 \text{ mV}$), the complexes bridged by dabco show very weak splits of 0–60 mV on the reduction waves obtained by CV.³⁶ In the porphyrin polymers aligned linearly, the Ru–oep–dabco complexes at carbon cloth electrodes showed no clear intramolecular redox interactions, and the potential split of the pz-bridged polymers were larger than in the bpy-bridged polymers,¹⁴ which should result from the difference in distance between two metal centers in each dimer. These results are consistent with the concept that conduction in the partially oxidized ruthenium-complex polymers occurs at metal center and the intramolecular redox interaction mainly reflects the extension of π -conjugated bridging ligand systems.^{14,37}

In the present carbonyl-coordinated porphyrin dimers, in the CV of the pz-bridged complexes of Os–ttp systems, there was a split in the first oxidation process and the bpy bridged complex exhibited no splits. The latter result is understandable due to the above reasons, that is, the intramolecular redox interaction of the bpy complex should be too small to observe a split in the potential. On the other hand, the results of the dabco system were surprising. Although the dabco complexes essentially have no π -conjugated system in the molecules and the distances between the two metal ions are a little larger than those of the pz complexes, the $[\{M(\text{ttp})(\text{CO})\}_2(\text{dabco})]$ complexes exhibited distinct intramolecular redox interactions with almost the same magnitude as that of the $[\{M(\text{ttp})(\text{CO})\}_2(\text{pz})]$ complexes. It has been reported that there are interactions between the two nitrogen atoms of a dabco molecule through the σ bond of the C–C linkage and the lone pair of the nitrogen atoms.³³ However, this concept does not explain the split as large as the pz porphyrin dimers at the first oxidation processes. A great many dabco systems have to be studied in order to make a definite conclusion.

Another striking result from the electrochemical studies is that the interaction intensities for ruthenium systems are comparable to the corresponding osmium systems, although these carbonyl-coordinated ruthenium and osmium complexes are redox active at the porphyrin rings and metal centers, respectively, in the first electrochemical oxidation process. This result suggests that the porphyrin ring-centered oxidation state of the ruthenium complexes can be distinguished from the metal-centered oxidation state, when electrons transfer to another site of a ruthenium porphyrin subunit through the bridging ligands. The effects of the porphyrin rings, the central metal ions, and the bridging ligands on the redox interactions go in the orders of $\text{ttp} > \text{oep}$ and $\text{Os}(\text{metal oxidation}) > \text{Ru}(\text{ring oxidation})$, and $\text{dabco} \geq \text{pz} \gg \text{bpy}$, respectively, though the oxidizing moieties in the first processes are different in the carbonyl-coordinated ruthenium and osmium porphyrin complexes. The order of $\text{ttp} > \text{oep}$ seems to reflect the difference in their redox potentials, that is, oep ring is oxidized more easily than ttp systems. These orders rationalize the result that the reported $[\{\text{Ru}(\text{oep})(\text{CO})\}_2(\text{BL})]$ systems exhibit no apparent splits.¹⁶ The separations must be <40 mV at the first oxidation processes. All of the dimer complexes in the present systems gave no corresponding pure mixed-valence complexes, because of the relative small potential splits. This made it impossible to study electron-molecular vibration coupling as observed in the 2-pyridylporphyrin dimer complexes.⁸ Since the axial CO ligand was thought to have large effects on the interaction of the present systems, we tried to prepare and isolate the dimer complexes with axial ligands, such as pyridine and 4-dimethylaminopyridine, instead of CO axial ligands, but we were unsuccessful in getting pure samples, though physicochemical measurements revealed the presence of the target complexes in the solutions. Instead, anthracene-bridged ruthenium porphyrin dimers with aza ligands at the axial positions are now being prepared.

Conclusion

Carbonyl-coordinated ruthenium(II) and osmium(II) porphyrin dimers bridged with aza-ligands of pz, bpy, and dabco

were prepared and characterized by using physicochemical measurements and X-ray crystallography. X-ray crystallography revealed that the central metal ions in the porphyrin subunits were located in each porphyrin plane and the distances between two metal ions were in the order of $\text{bpy} \gg \text{dabco} \geq \text{pz}$. All these complexes exhibited blue-shifted Soret bands compared to the corresponding monomers, which indicates the presence of intramolecular interactions in the cofacial porphyrin dimers. Electrochemical measurements also demonstrated that, in both of the ruthenium and osmium porphyrin dimers, the pz and dabco complexes exhibited intramolecular redox interactions, as observed by the split in each of the waves for the first oxidation processes. The bpy complex had no splits as was expected from the distance between two metal ions. The interaction of the dabco complexes, which have no π -conjugated system or have only a small amount of conjugation between two nitrogen atoms through C–C bonds in dabco, was not so different from that of the pz complex, which has a π conjugation system in the molecule. In addition, no essential difference in the magnitude of the intramolecular redox interactions was observed between ruthenium and osmium complex systems, though in the former, the first oxidation occurred at the porphyrin rings, and in the latter, the oxidation occurred at the metal centers.

Supporting Information

The arrangement of $[\{\text{Os}(\text{ttp})(\text{CO})\}_2(\text{pz})]$ molecules in the a–c plane (Fig. S1) and plots of difference between two peaks (mV) obtained by DPV vs. HWHM (full-width at the half-maximum from the top) at the first oxidation processes (Fig. S2). These material are available free of charge on the web at <http://www.csj.jp/journals/bcsj/>.

References

- 1 a) J.-H. Chou, M. E. Kosal, H. S. Nalwa, N. A. Rakow, K. S. Suslick, in *The Porphyrin Handbook*, ed. by K. M. Kadish, K. M. Smith, R. Guilard, Academic Press, New York, **2000**, Vol. 6, Chap. 41, p. 43. b) C. M. Drain, J. T. Hupp, K. S. Suslick, M. R. Wasielewski, X. Chen, *J. Porphyrins Phthalocyanines* **2002**, 6, 243.
- 2 M. L. Merlau, M. del P. Mejia, S.-B. Nguyen, J. T. Hupp, *Angew. Chem., Int. Ed.* **2001**, 40, 4239.
- 3 a) H. Ogoshi, T. Mizutani, T. Hayashi, Y. Kuroda, in *The Porphyrin Handbook*, ed. by K. M. Kadish, K. M. Smith, R. Guilard, Academic Press, New York, **2000**, Vol. 6, Chap. 46, p. 279. b) D. M. Vriezema, M. C. Aragones, J. A. A. W. Elemans, J. J. L. M. Cornelissen, A. E. Rowan, R. J. M. Nolte, *Chem. Rev.* **2005**, 105, 1445. c) J. K. M. Sanders, in *The Porphyrin Handbook*, ed. by K. M. Kadish, K. M. Smith, R. Guilard, Academic Press, New York, **2000**, Vol. 3, Chap. 22, p. 347.
- 4 a) D. Gust, T. A. Moore, in *The Porphyrin Handbook*, ed. by K. M. Kadish, K. M. Smith, R. Guilard, Academic Press, New York, **2000**, Vol. 8, Chap. 57, p. 153. b) F. Hajjaj, Z. S. Yoon, M.-C. Yoon, J. Park, A. Satake, D. Kim, Y. Kobuke, *J. Am. Chem. Soc.* **2006**, 128, 4612. c) P. D. Harvey, in *The Porphyrin Handbook*, ed. by K. M. Kadish, K. M. Smith, R. Guilard, Academic Press, New York, **2003**, Vol. 18, p. 63. d) M.-S. Choi, T. Yamazaki, I. Yamazaki, T. Aida, *Angew. Chem., Int. Ed.* **2004**, 43, 150. e) D. Kim, A. Osuka, *Acc. Chem. Res.* **2004**, 37, 735. f) T. S. Balaban, *Acc. Chem. Res.* **2005**, 38, 612. g) D. Holten,

D. F. Bocian, J. S. Lindsey, *Acc. Chem. Res.* **2002**, *35*, 57.

5 J.-L. Chambron, V. Heitz, J.-P. Sauvage, in *The Porphyrin Handbook*, ed. by K. M. Kadish, K. M. Smith, R. Guilard, Academic Press, New York, **2000**, Vol. 6, Chap. 40, p. 1.

6 a) T. Imamura, K. Fukushima, *Coord. Chem. Rev.* **2000**, *198*, 133. b) J. Wojaczynski, L. Latos-Grazynski, *Coord. Chem. Rev.* **2000**, *204*, 113.

7 K. Funatsu, T. Imamura, A. Ichimura, Y. Sasaki, *Inorg. Chem.* **1998**, *37*, 4986.

8 T. Imamura, K. Funatsu, S. Ye, Y. Morioka, K. Uosaki, Y. Sasaki, *J. Am. Chem. Soc.* **2000**, *122*, 9032.

9 V. Marvaud, J.-P. Launay, *Inorg. Chem.* **1993**, *32*, 1376.

10 a) O. Schneider, J. Metz, M. Hanack, *Mol. Cryst. Liq. Cryst.* **1982**, *81*, 273. b) M. Hanack, *Mol. Cryst. Liq. Cryst.* **1984**, *105*, 133.

11 R. S. Nohr, P. M. Kuznesof, K. J. Wynne, M. E. Kenney, P. G. Siebenman, *J. Am. Chem. Soc.* **1981**, *103*, 4371.

12 a) B. N. Diel, T. Inabe, N. K. Jaggi, J. W. Lyding, O. Schneider, M. Hanack, C. R. Kannewurf, T. J. Marks, L. H. Schwartz, *J. Am. Chem. Soc.* **1984**, *106*, 3207. b) C. W. Dirk, T. Inabe, K. F. Schoch, Jr., T. J. Marks, *J. Am. Chem. Soc.* **1983**, *105*, 1539.

13 J. P. Collman, J. T. McDevitt, G. T. Yee, C. R. Leidner, L. G. McCullough, W. A. Little, J. B. Torrance, *Proc. Natl. Acad. Sci. U.S.A.* **1986**, *83*, 4581.

14 J. P. Collman, J. T. McDevitt, C. R. Leidner, G. T. Yee, J. B. Torrance, W. A. Little, *J. Am. Chem. Soc.* **1987**, *109*, 4606.

15 Abbreviations: ttp = 5,10,15,20-tetra-*p*-tolylporphyrinato dianion; oep = 2,3,7,8,12,13,17,18-octaethylporphyrinato dianion; py = pyridine; mpy = 4-methylpyridine; pz = pyrazine; bpy = 4,4'-bipyridine; dabco = 1,4-diazabicyclo[2,2,2]octane; TBAP = tetrabutylammonium perchlorate; TBA(PF₆) = tetrabutylammonium hexafluorophosphate; DDQ = 2,3-dichloro-5,6-dicyano-1,4-benzoquinone; CV = Cyclic Voltammetry; DPV = Differential Pulse Voltammetry.

16 A. Endo, Y. Okamoto, K. Suzuki, J. Shimamura, K. Shimizu, G. P. Sato, *Chem. Lett.* **1994**, 1317. Carbonyl-coordinated [{Ru(oep)(CO)}₂(BL)] showed two oxidation processes. Each of these two oxidation processes involved two-electron transfers. However, the splits in each oxidation process have not been reported, because they are very small, though stepwise one-electron transfers at the first oxidation process have been suggested.

17 D. P. Rillema, J. K. Nagle, L. F. Barringer, Jr., T. J. Meyer, *J. Am. Chem. Soc.* **1981**, *103*, 56.

18 G. M. Brown, F. R. Hopf, T. J. Meyer, D. G. Whitten, *J. Am. Chem. Soc.* **1975**, *97*, 5385.

19 *CrystalClear*, Rigaku Co., **1999**.

20 *CrystalStructure 3.6.0: Crystal Structure Analysis Package*, Rigaku and Rigaku/MSO, 9009 New Trails Dr., The Woodlands TX 77381, U.S.A., **2000–2004**.

21 G. M. Sheldrick, *SHELXL-97, Program for the Refinement of Crystal Structures*, University of Göttingen, Germany, **1997**.

22 J. P. Collman, C. E. Barnes, P. J. Brothers, T. J. Collins, T. Ozawa, J. C. Gallucci, J. A. Ibers, *J. Am. Chem. Soc.* **1984**, *106*, 5151.

23 a) A. Antipas, J. W. Buchler, M. Gouterman, P. D. Smith, *J. Am. Chem. Soc.* **1978**, *100*, 3015. b) W. Sovocool, E. R. Hopf, D. G. Whitten, *J. Am. Chem. Soc.* **1972**, *94*, 4350.

24 C.-M. Che, C.-K. Poon, W.-C. Chung, H. B. Gray, *Inorg. Chem.* **1985**, *24*, 1277.

25 K. Funatsu, A. Kimura, T. Imamura, A. Ichimura, Y. Sasaki, *Inorg. Chem.* **1997**, *36*, 1625.

26 The hydrogen atoms were located at the calculated position. An acceptable *R* value and the normal shape of tolyl groups allowed the evaluation of H...H distance.

27 Because ethyl groups showed disorder and because the terminal methyl groups can rotate around the C–C bonds, not the H...H distance but the C...C distance was used for discussion of the oep complexes.

28 In this setting, the minimum H...H separation becomes 2.20 Å if mirror symmetry is supposed. However, the ethyl group is flexible and the small rotation of terminal methyl group can evade such close contact.

29 N. Kariya, T. Imamura, Y. Sasaki, *Inorg. Chem.* **1997**, *36*, 833.

30 J. W. Buchler, K. Rohbock, *J. Organomet. Chem.* **1974**, *65*, 223.

31 a) M. Kasha, H. L. Rawls, M. A. El-Bayoumi, *Pure Appl. Chem.* **1965**, *11*, 371. b) M. Kasha, *Radiat. Res.* **1963**, *20*, 55.

32 S. Vagin, U. Ziener, M. Hanack, P. Stuzhin, *Eur. J. Inorg. Chem.* **2004**, 2877.

33 a) R. Hoffmann, *Acc. Chem. Res.* **1971**, *4*, 1. b) M. H. Paddon-Row, *Acc. Chem. Res.* **1982**, *15*, 245. c) E. Heilbronner, K. A. Muszkat, *J. Am. Chem. Soc.* **1970**, *92*, 3818.

34 R. Hoffmann, A. Imamura, W. J. Hehre, *J. Am. Chem. Soc.* **1968**, *90*, 1499.

35 C. Creutz, H. Taube, *J. Am. Chem. Soc.* **1973**, *95*, 1086.

36 T. Ito, T. Yamaguchi, C. P. Kubiak, *Macromol. Symp.* **2000**, *156*, 269.

37 J. P. Collman, J. T. McDevitt, G. T. Yee, M. B. Zisk, J. B. Torrance, W. A. Little, *Synth. Met.* **1986**, *15*, 129, and references therein.